1997 ASME Fluids Engineering Division Summer Meeting
FEDSM'97
June 22 - 26, 1997

FEDSM97-3228

FLUIDIC THRUST VECTORING OF AN AXISYMMETRIC EXHAUST NOZZLE AT STATIC CONDITIONS

David J. Wing
NASA Langley Research Center
Hampton, VA

Victor J. Giuliano
Pratt & Whitney
West Palm Beach, FL

ABSTRACT

A sub-scale experimental static investigation of an axisymmetric nozzle with fluidic injection for thrust vectoring was conducted at the NASA Langley Jet Exit Test Facility. Fluidic injection was introduced through flush-mounted injection ports in the divergent section. Geometric variables included injection-port geometry and location. Test conditions included a range of nozzle pressure ratios from 2 to 10 and a range of injection total pressure ratio from no-flow to 1.5.

The results indicate that fluidic injection in an axisymmetric nozzle operating at design conditions produced significant thrust-vector angles with less reduction in thrust efficiency than that of a fluidically-vectored rectangular jet. The axisymmetric geometry promoted a pressure relief mechanism around the injection slot, thereby reducing the strength of the oblique shock and the losses associated with it. Injection port geometry had minimal effect on thrust vectoring.

NOMENCLATURE

$C_{f,g_{sys}}$	system resultant thrust coefficient, $\frac{\sqrt{F_a^2 + F_n^2}}{F_{i,p} + F_{i,s}}$
F_a	thrust measured along nozzle axis, lbf
$F_{i,p}$	ideal isentropic thrust of primary jet, lbf,
$F_{i,s}$	ideal isentropic thrust of injection stream, lbf,
F_n	measured normal force, lbf
JETF	Jet Exit Test Facility
NPR	nozzle pressure ratio, $p_{t,j}/p_a$
p	local internal static pressure, psia
p_a	atmospheric pressure, psia
$p_{t,j}$	average primary jet total pressure, psia
$p_{t,s}$	injection stream total pressure, psia
SPR	secondary total pressure ratio, $p_{t,s}/p_{t,j}$
$T_{t,j}$	primary jet total temperature, °R
$T_{t,s}$	injection stream total temperature, °R
w_p	primary weight flow rate, lbf/sec
w_s	injection stream weight flow rate, lbf/sec
x	axial distance measured from nozzle throat (fig. 1), in.
δ_v	thrust-vector angle, deg., $\tan^{-1}(F_n/F_a)$
θ	angular coordinate of nozzle (fig. 1), deg.
$\omega\sqrt{\tau}$	corrected weight flow rate of injection stream, $\frac{w_s}{w_p}\sqrt{\frac{T_{t,s}}{T_{t,j}}}$

Introduction

Thrust-vector control via secondary injection for rocket propulsion systems has been investigated since the 1950's. The Polaris missile utilized a secondary injection system in its axisymmetric exhaust nozzle for thrust-vector control. Recent investigations have explored the benefits of fluidic nozzle control for air-breathing propulsion systems and have found that significant thrust-vector angles could be generated by injecting a secondary airstream into the divergent section of a nozzle (Wing, 1994). By using fluidic control in place of mechanical control, significant portions of the nozzle hardware could be structurally integrated (i.e. fixed) with the non-moving airframe structure. This integration would allow the elimination of the kinematic structure and mechanical actuators, and may result in a significant reduction in nozzle weight, cost, and complexity. Although fluidic thrust-vector control of several nozzles with non-axisymmetric cross-sectional geometries (e.g. rectangular, triangular, hexagonal) has been investigated (mostly

unpublished) and fluidic throat-area control of axisymmetric nozzles has been investigated (Catt et al.), the axisymmetric nozzle has yet to be adequately explored for its potential in fluidic thrust-vector control for air-breathing propulsion systems. A fluidic thrust-vectoring nozzle with axisymmetric geometry has the benefits of structural efficiency and the possibility of retrofit onto existing aircraft.

A sub-scale experimental static investigation of an axisymmetric nozzle with fluidic injection for thrust vectoring was conducted at the NASA Langley Jet Exit Test Facility. Fluidic injection was introduced through flush-mounted injection ports in the divergent section. Variations on the injection port design included slot longitudinal location, number of slots, and a distributed pattern of holes rather than slots. Test conditions included a range of nozzle pressure ratios (*NPR*) from 2 to 10 and a range of injection total pressure ratio (*SPR*) from no-flow to 1.5. Measurements included normal and axial forces and internal static pressures distributed over a 180° arc-sector of the nozzle (nearly full internal coverage due to symmetry) extending from upstream of the nozzle throat to the nozzle trailing edge. A paint flow visualization technique was applied for selected configurations and test conditions: an oil-based paint was applied to the divergent-duct internal surface and allowed to dry at constant nozzle operating conditions. The dried paint patterns indicate flow features at the nozzle surface.

Model Description

The model was a 10 percent-scale axisymmetric nozzle with a throat area of 3.736 in^2 and an expansion ratio (exit area divided by throat area) of 1.738. Two independently-operated injection ports were located in opposing sectors of the divergent duct for fluidic thrust vectoring. For the data presented in this paper, only one port was flowing; the other port existed only as a closed cavity. An additional aspect of this experiment (not reported on here) was the investigation of symmetric injection for expansion control, where both slots were flowing.

A sketch of the model hardware is shown in figure 1. The main hardware components consisted of a convergent section, a throat-block insert, an injection plenum disk, several pairs of interchangeable injection-port inserts, and a plenum cover. The injection plenum disk contained two isolated 90°-sector opposing plenums for fluidic injection. Each plenum contained a baffle plate for even pressure distribution and three static pressure taps for plenum pressure measurement. The plenums were designed to accept interchangeable inserts for variations in injection-port geometry. The injection-port geometry variations included slot axial location (forward or aft), numbers of slots (single or triple), and a distributed hole pattern rather than slots. All of the injection ports were tested with injection flow delivered across an arc angle of 60° (±30° off θ=0°).

The nozzle internal surface was instrumented with 57 static pressure orifices arranged in seven longitudinal rows spaced 30° apart, with θ=0° centered on the upper (flowing) injection slot. The orifice rows extended from just upstream of the nozzle throat to near the trailing edge, resulting in nearly complete coverage of the internal divergent duct due to nozzle symmetry.

Facility Description

The test was conducted in the NASA Langley Jet Exit Test Facility (JETF). The facility is used for static performance testing of scaled nozzle concepts and is capable of supplying multiple flows to the nozzle. The JETF consists of two independently supplied and controlled high-pressure air lines, a dual-flow propulsion simulation stand (shown in figure 2), and a data acquisition system. Each air supply can be continuously regulated up to approximately 23 lbf/sec. The air supply is maintained at approximately 535°R during testing, and the flow is exhausted through the nozzle to atmospheric pressure in a large, vented room. Further information on the JETF can be found in NASA-TM-102750 (see References).

Results and Discussion

Overexpanded Primary Jet

The system resultant thrust coefficient ($C_{f,g_{sys}}$), based on the sum of the ideal thrusts of the primary and injected flow, and the thrust-vector angle (δ_v) of the aft-slot configuration as functions of secondary weight flow ratio ($\omega\sqrt{\tau}$) for *NPR*=3 and *NPR*=8.26 are presented in figure 3. The lower *NPR* represents a low-speed operating condition such as takeoff or high angle-of-attack flight where thrust vectoring might be used to supplement or replace the conventional aerodynamic controls. The higher *NPR* is the design pressure ratio for this configuration (based on the exit-to-throat-area expansion ratio) where thrust vectoring might be used for trim-drag reduction at cruise operating conditions.

At *NPR*=3, the nozzle was producing thrust at a relatively low performance level ($C_{f,g_{sys}}$=0.895), expected behavior of a nozzle operating at significantly overexpanded flow conditions. In an operational nozzle, additional steps would be taken to ensure that the nozzle thrust efficiency would be raised to higher levels (such as the fluidic expansion control technique also investigated in this experiment, but not reported on in this paper). At the lower *NPR*, thrust-vector angles of up to δ_v=18° were generated with mainly positive impact on system resultant thrust coefficient. For $\omega\sqrt{\tau} \leq 0.08$, an increase in performance over that for no injection was measured.

The pressure distribution at *NPR*=3 is shown in figure 4; the solid symbols represent the "clean" nozzle configuration with no injection slots, and the open symbols represent the aft-slot configuration at a secondary pressure ratio (*SPR*) of 1. The

pressure distribution of the clean configuration indicates that the majority of the divergent duct was at sub-ambient conditions and a shock (sudden or discontinuous increase in pressure) was formed at approximately x=1.5 in., consistent with the expected flow separation characteristic, to re-pressurize the flow to ambient conditions. (Note that the dashed line indicates the estimated pressure distribution at the shock location). For the injected flow case, a pressurized region formed upstream of the injection slot (θ=0° and 30°) and a sub-ambient region dominated the opposite regions of the nozzle (θ>90°); the integrated effect of these pressure distributions is the net vertical force component of the vectored thrust. Also, no similar shock is evident (although no pressure measurements were obtained near the trailing edge for θ>120°). Therefore, since much of the drag-producing sub-ambient pressure region was eliminated, the injected flow resulted in an increase in thrust efficiency of the primary jet. As shown in figure 3, this increase in thrust efficiency was accomplished at the smallest injection flow rate. Further increases in injection flow rate resulted in a decrease in system thrust efficiency. This was probably the result of a combination of the injected stream itself losing efficiency as it operated at ever-increasing underexpanded conditions (the injection slot was essentially a convergent nozzle) and increasing (with increasing injection pressure ratio) thrust losses associated with turning of the injected flow once its maximum penetration into the primary stream was achieved.

An additional flow feature is illustrated in figure 4. A circumferential pressure gradient was created immediately downstream of the geometric throat (x=0.1 in.), with the highest pressure in line with the injection slot (θ=0°) and diminishing pressure outboard of this location (θ increasing to 90°). This gradient redirected some of the primary exhaust around the injection slot to the outboard upper regions of the nozzle (θ = 60° and 90°), thereby providing a pressure relief mechanism for the primary exhaust. This relief possibly alleviated the need for the formation of a strong oblique shock in front of the injection slot. Strong shocks just forward of the injection region have been seen for two-dimensional flow fields of injection into a supersonic stream (Aso, et al., 1991, and Wing, 1994). The relief mechanism, in combination with the smooth contours of the axisymmetric duct, may have also allowed a gradual shock-free pressure recovery to near-ambient conditions to occur in the side regions of the nozzle (θ = 60°, 90°, and 120°).

A flow visualization photograph of the aft-slot configuration showing surface flow patterns at *NPR*=3 and *SPR*=1 is presented in figure 5. Paint streaks indicate that flow originating from the pressurized region upstream of the injection slot was diverted around the injection slot and directed out the nozzle exit at an angle indicative of a deflected jet. The influence of the injected flow on the surface flow patterns appears to extend around the nozzle to approximately θ=120°, where the flow patterns indicate a strong normal shock similar to that indicated by the clean-configuration pressure distribution at x=1.5 (fig. 4); this range of influence of the injection is consistent with the pressure distribution, where the pressure ratios at θ=120° deviate only slightly from those of the clean nozzle configuration (slightly higher pressures were measured and no shock was seen).

Fully-Expanded Primary Jet

As seen in figure 3 for the no injection flow case ($\omega\sqrt{\tau}$ =0), resultant thrust ratio was 7.6 percent higher at *NPR*=8.26 (design condition) than at *NPR*=3, illustrating that overexpansion losses had been eliminated. At *NPR*=8.26, resultant thrust ratio was adversely affected by increased secondary injection flow rate. Internal static pressure distributions of the nozzle at *NPR*=8.26 are shown in figure 6; the solid symbols represent the clean configuration with no injection slots, and the open symbols represent the aft-slot configuration at *SPR*=1. As can be seen for the clean configuration, no areas of sub-ambient pressure exist in the divergent duct. In general, the pressure distribution was similar to that for *NPR*=3 (fig. 4); however, the increases in pressure along orifice rows θ=30°, 60°, 90°, and 120° indicated an apparent discontinuity in pressure which occurred at successively further downstream locations with increasing θ, indicating the possible presence of an internal oblique shock. The distribution at θ=120° was nearly identical to that of the clean configuration except for the last pressure orifice, indicating that the shock probably exited the nozzle in this vicinity and the injection did not likely affect the flow field for θ>120°. At this fully-expanded design *NPR*, the primary jet would not be able to take advantage of the pressure relief offered by overexpanded regions to adjust to the injection flow with such minimal thrust losses seen at *NPR*=3; a shock would therefore be required to turn the flow, resulting in more significant losses in thrust performance.

A flow visualization photograph of the aft-slot configuration at *NPR*=8.26 and *SPR*=1 is shown in figure 7. The flow patterns are more difficult to see because the higher flow velocity resulted in the removal of most of the paint before it was able to dry. As was seen for *NPR*=3 (fig. 5), the patterns indicate a circumferential direction of flow from the pressurized region upstream of the slot to the outboard regions of the nozzle. Careful inspection of the original photographs revealed that these deflected flow patterns only occurred downstream of an oblique cut through the nozzle, which would be consistent with the existence of an oblique shock, as discussed above. The circumferential pressure gradient shown in figure 6 diverted the primary exhaust to the outboard regions of the nozzle, pressurizing these regions. As will be further discussed in the next section, the thrust-vector angle could be adversely affected when these high pressure regions extend beyond θ = 90°.

The thrust vectoring performance of a rectangular nozzle with divergent-flap injection was documented by Wing (1994).

Interpolation of that database indicated a loss in resultant thrust coefficient for the rectangular nozzle of approximately 4.3 percent at $\omega\sqrt{\tau} = 0.1$, whereas the axisymmetric nozzle incurred only a 3.1 percent loss at the same conditions (also through interpolation). The greater efficiency in thrust vectoring for the axisymmetric nozzle may be related to the pressure relief mechanism discussed earlier and the apparent reduction in the oblique shock strength needed for the primary jet to negotiate the obstruction of the injected flow. The rectangular nozzle had no such relief mechanism since the slot spanned the nozzle width, possibly requiring the formation of a stronger oblique shock with greater losses.

Effect of Slot Geometry

In figure 8, the thrust vectoring performance of the nozzle at *NPR*=3 is shown with four different injection port geometries: aft slot, forward slot, triple slot, and distributed hole pattern. All four configurations produced similar levels of thrust vectoring with only minor differences. The forward-slot configuration generally produced slightly greater thrust-vector angles than the other configurations. A comparison of the flow visualization photograph of the forward-slot configuration in figure 9 with that of the aft slot configuration in figure 5 indicates that the primary exhaust in front of the forward slot was diverted earlier and to a farther extent around the nozzle, tending to pressurize the lower half of the nozzle and reduce the thrust-vector angle. However, the overexpansion shock near the trailing edge opposite the flowing injection slot was shifted aft as the slot was shifted forward, reducing the size of the higher pressure region aft of the shock, and thereby increasing the thrust-vector angle. These two changes in pressure distribution with changes in slot location have opposing effects on the thrust-vector angle, indicating that an optimum slot position exists for thrust vectoring at a given set of primary and secondary flow conditions.

If the slot is moved further forward or the injection flow rate is increased, the overexpansion shock would eventually disappear and the increased pressure on the lower-half of the nozzle from the diverted flow would begin to reduce the thrust-vector angle. An example of this condition is seen in figure 8, where the thrust-vector angle for the forward slot configuration diminished as $\omega\sqrt{\tau}$ was increased from 0.08 to 0.12. A flow visualization photograph (not shown) confirmed that the overexpansion shock had disappeared at this condition, and the surface flow patterns extended farther around the nozzle.

The thrust vectoring performance of the two remaining configurations, the triple-slot and distributed-hole-pattern injection ports, are also shown in figure 8 but will not be discussed in detail. The triple-slot configuration generally produced slightly smaller thrust-vector angles than the other configurations, and the distributed hole pattern produced thrust-vector angles generally similar to the aft-slot configuration. However, neither configuration exhibited any significant beneficial or detrimental thrust-vectoring behavior as compared to the single-slot geometry. The data confirms that both configurations are viable injection port designs for fluidic thrust vectoring.

Conclusions

A sub-scale experimental static investigation of an axisymmetric nozzle with fluidic injection for thrust vectoring was conducted at the NASA Langley Jet Exit Test Facility. Fluidic injection was introduced through flush-mounted injection ports in the divergent section. Geometric variables included injection-port geometry and location. Test conditions included a range of nozzle pressure ratios from 2 to 10 and a range of injection total pressure ratio from no-flow to 1.5. Based on the discussion of results, the following conclusions are highlighted:

1) At an overexpanded operating condition, fluidic thrust vectoring of the axisymmetric jet up to 18° was accomplished with some beneficial effect on thrust efficiency. At the primary-jet design operating condition, a lower level (up to 13°) of thrust vectoring was accomplished, but with significantly lower losses in thrust efficiency when compared to a rectangular jet at similar conditions. The smooth and continuous contours of the axisymmetric duct allowed an efficient pressure relief to occur around the injection slot, thereby reducing the strength of the oblique shock system and the loss in thrust efficiency.

2) Injection port geometry had only minor effects on the generation of thrust-vector angle. At overexpanded primary jet conditions, moving the injection port forward generally increased the thrust-vector angle by reducing the separated region opposite the injection near the trailing edge. However, pressure levels in the lower half of the duct were also increased because of the pressure relief mechanism, stated in conclusion #1, which detracted from the thrust-vector angle.

REFERENCES

Aso, S.; Okuyama, S.; and Ando, Y., 1991, "Experimental Study on Interacting Flow Fields Induced by Normally Injected Secondary Flow Through a Slot Nozzle Into Supersonic Flow," Memoirs Faculty Eng., Kyushu Univ., vol. 51, no. 1, pp. 53-62.

Catt, J. A.; Miller, D. N.; Giuliano, V. J., 1995, "A Static Investigation of Fixed-Geometry Nozzles Using Fluidic Injection for Throat Area Control," AIAA 95-2604.

Staff of the Propulsion Aerodynamics Branch, 1990, "A User's Guide to the Langley 16-Foot Transonic Tunnel Complex, Revision 1," NASA TM-102750.

Wing, D. J., 1994, "Static Investigation of Two Fluidic Thrust-Vectoring Concepts on a Two-Dimensional Convergent-Divergent Nozzle. NASA TM-4574.

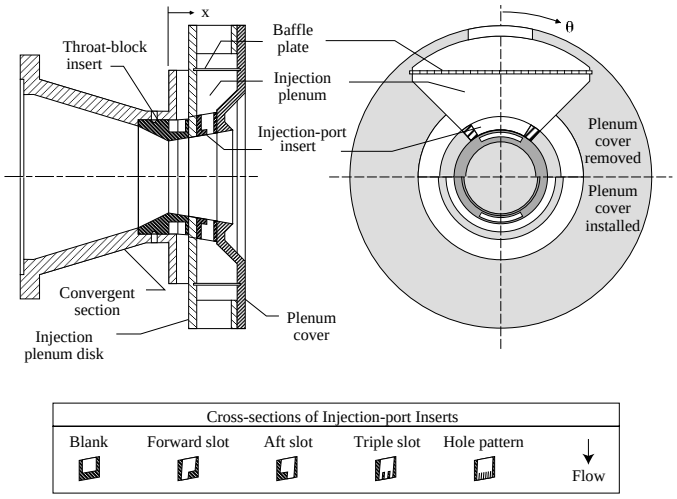

Figure 1. Sketch of the fluidic axisymmetric nozzle model.

Figure 2. Dual-flow propulsion simulation stand with the fluidic axisymmetric nozzle installed.

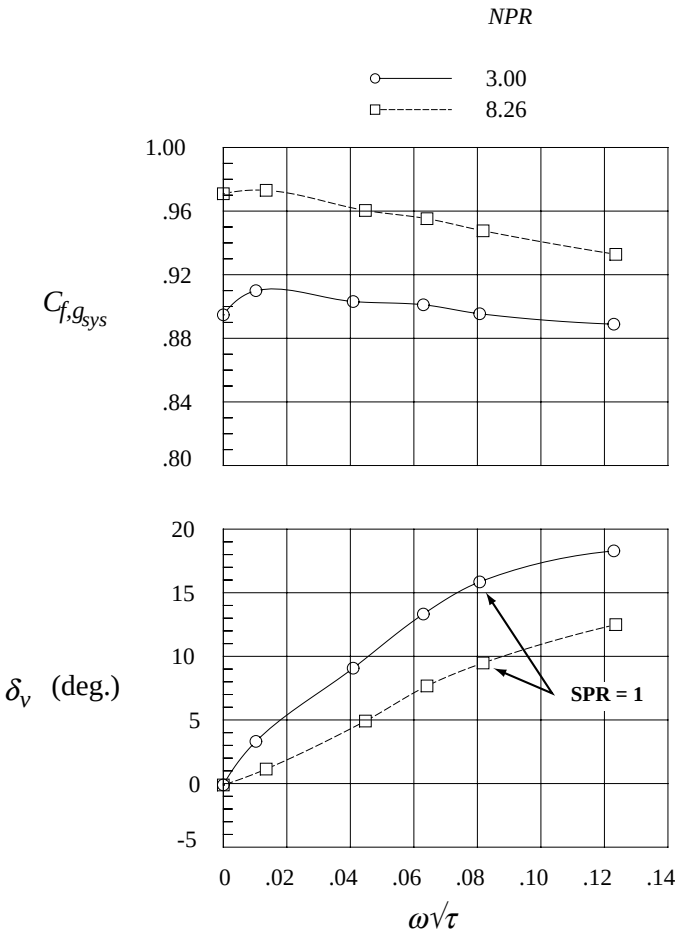

Figure 3. Resultant thrust efficiency and thrust-vectoring performance of the aft-slot configuration.

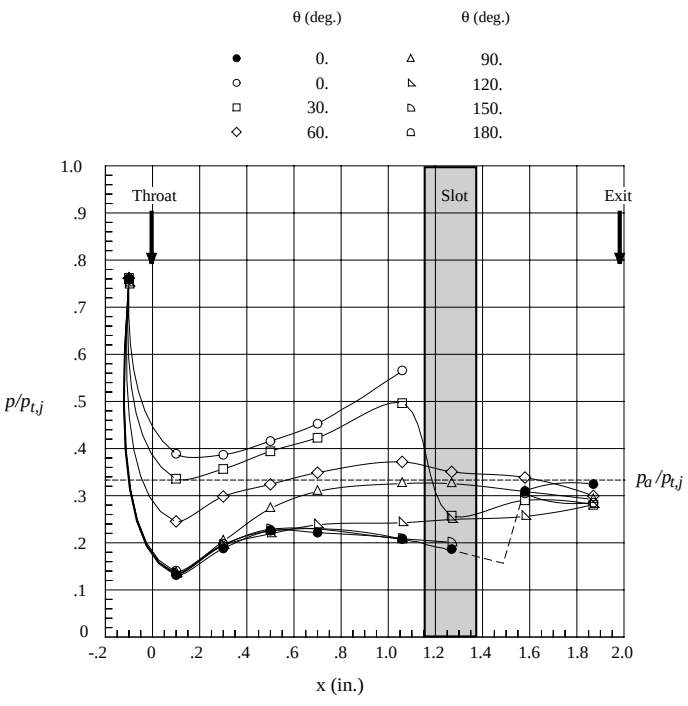

Figure 4. Static pressure distribution of the aft-slot configuration at *NPR*=3 and *SPR*=1. Solid symbols indicate the clean configuration.

Figure 5. Flow visualization of the aft-slot configuration at *NPR*=3 and *SPR*=1.

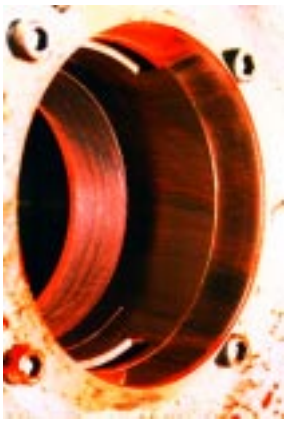

Figure 7. Flow visualization of the aft-slot configuration at *NPR*=8.26 and *SPR*=1.

Figure 9. Flow visualization of the forward-slot configuration at *NPR*=3 and *SPR*=1.

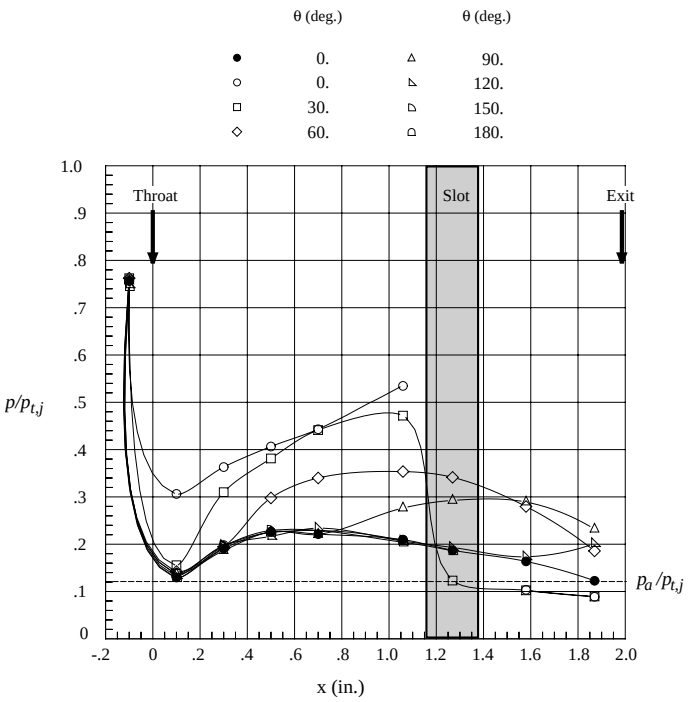

Figure 6. Static pressure distribution of the aft-slot configuration at *NPR*=8.26 and *SPR*=1. Solid symbols indicate the clean configuration.

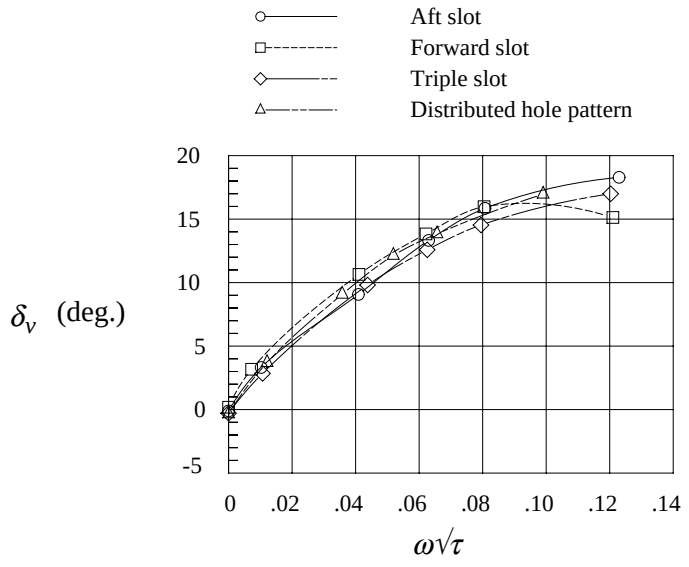

Figure 8. Effect of injection-port geometry on thrust-vectoring performance at *NPR*=3.